ELSEVIER

Earth and Planetary Science Letters 150 (1997) 413–425

EPSL

Erosion rates of alpine bedrock summit surfaces deduced from in situ ^{10}Be and ^{26}Al

Eric E. Small [a,*], Robert S. Anderson [a], James L. Repka [a], Robert Finkel [b]

[a] *Department of Earth Sciences and Institute for Tectonics, University of California, Santa Cruz, CA 95064, USA*
[b] *Center for Accelerator Mass Spectrometry, Lawrence Livermore National Laboratory, Livermore, CA 94551, USA*

Received 13 September 1996; revised 9 May 1997; accepted 9 May 1997

Abstract

We have measured the concentration of in situ produced cosmogenic ^{10}Be and ^{26}Al from bare bedrock surfaces on summit flats in four western U.S. mountain ranges. The maximum mean bare-bedrock erosion rate from these alpine environments is 7.6 ± 3.9 m My^{-1}. Individual measurements vary between 2 and 19 m My^{-1}. These erosion rates are similar to previous cosmogenic radionuclide (CRN) erosion rates measured in other environments, except for those from extremely arid regions. This indicates that bare bedrock is not weathered into transportable material more rapidly in alpine environments than in other environments, even though frost weathering should be intense in these areas. Our CRN-deduced point measurements of bedrock erosion are slower than typical basin-averaged denudation rates (~ 50 m My^{-1}). If our measured CRN erosion rates are accurate indicators of the rate at which summit flats are lowered by erosion, then relief in the mountain ranges examined here is probably increasing.

We develop a model of outcrop erosion to investigate the magnitude of errors associated with applying the steady-state erosion model to episodically eroding outcrops. Our simulations show that interpreting measurements with the steady-state erosion model can yield erosion rates which are either greater or less than the actual long-term mean erosion rate. While errors resulting from episodic erosion are potentially greater than both measurement and production rate errors for single samples, the mean value of many steady-state erosion rate measurements provides a much better estimate of the long-term erosion rate. © 1997 Elsevier Science B.V.

Keywords: erosion rates; frost action; cosmogenic radionuclides; weathering; alpine environment

1. Introduction

The measurement of erosion and weathering rates, in different geomorphic settings and across various temporal and spatial scales, is essential to the quantification of rates and styles of landscape evolution, the understanding of the controls and efficiencies of different geomorphic processes, and the establishment of connections between climate change and landscape response. At present, the analysis of in situ produced cosmogenic radionculides (CRNs) is the only way to quantify long-term average ($> 10^3$–10^4 yr) erosion rates of bare bedrock surfaces [1,2]. The rate at which a rock surface is lowered relative to some datum (the erosion rate) is not the only valuable geomorphic information that can be learned from cosmogenic erosion rate analyses. In addition,

* Corresponding author. E-mail: esmall@earthsci.ucsc.edu

PII S0012-821X(97)00092-7

the rate at which bare bedrock is transformed into transportable material (the weathering rate) can also be measured. This is possible because the rock surfaces sampled for cosmogenic erosion rate analyses are bare bedrock, which indicates that local erosion must have kept pace with the production of transportable material by weathering processes. At weathering-limited sites such as these, the erosion rate is limited by the weathering rate, and the two rates must be equal.

Previously reported CRN erosion rates span a wide range (0.1–100 m My^{-1}) (Table 1). This variability is not surprising because measurements have been made from various lithologies and in different environments. Erosion rates measured in Antarctica and Australia are much lower (0.1–1 m My^{-1}) than rates measured elsewhere, which has been attributed to the extreme aridity of these regions [3,4]. With the exception of CRN erosion rates measured from several alpine sites, rates from less arid areas fall within a narrow range, and appear to be independent of rock type ($\sim$ 5–10 m My^{-1}) (Table 1). The few erosion rates measured in alpine settings are noticeably faster (8, 14, 48 and 56 m My^{-1}) [5], which could indicate that frost action accelerates mechanical weathering. Previous frost-weathering studies have not established the efficiency of frost weathering in transforming bedrock into transportable material, relative to other weathering processes [6–15]. Additional CRN erosion rate measurements are needed to more fully assess the efficiency of frost weathering.

In this study we report bare-bedrock erosion rates, and therefore weathering rates, from alpine environments (above treeline), deduced from concentrations of the CRNs ^{10}Be and ^{26}Al. Our measurements are useful for evaluating the relative efficiency of frost action as a physical weathering process, quantifying spatial variations in erosion rates within high relief regions, and examining if CRN-deduced erosion rates from rock surfaces in alpine environments are slower than basin-averaged denudation rates in similar settings. In addition, we develop a model to investigate the magnitude of errors associated with applying the steady-state erosion model to episodically eroding outcrops. This model is broadly useful because the steady erosion assumption, which is fundamental for deducing erosion rates from CRN concentrations, cannot be tested in most geomorphic settings. We use results from this model to evaluate our erosion rate measurements and recommend a sampling scheme that minimizes errors resulting from episodic erosion.

Table 1
Previously reported CRN erosion rates measured from bare bedrock surfaces

Location	Rock type	Erosion rate (m My^{-1})	Climate	Author
Mt. Evans (CO)	granite	8 [a]	alpine	Nishizumi et al. [5]
Grand Tetons (WY)	granodiorite	48 [a]	alpine	
Himalayas	granodiorite	14 [a], 56 [a]	alpine	
Georgia Piedmont (GA)	granite	8	temperate	Bierman [38]
Llano Uplift (TX)	granite	12	semi-arid	
Alabama Hills (CA)	granite	7	semi-arid	
Haleakala and Mauna Loa (HW)	basalt	7–11	various (0–3 km elev.)	Kurz [39]
Pajarito Plateau (NM)	tuff	1–10	temperate	Albrecht et al. [40]
Eyre Peninsula, Australia	granite	0.5–1.0	semi-arid	Bierman and Turner [4]
Antarctica	sandstone	0.1–1.0	hyper-arid	Nishiizumi et al. [3]
Fort Sage Mtns. (CA)	granodiorite	50 [b]	semi–arid	Granger et al. [27]
Luquillo Experimental	quartz diorite	43 [b], 25 [a]	lower montane	Brown et al. [26]

Erosion rates from studies in which only several measurements were completed are not summarized here. The lithology and climate of each study area is described. The final two entries [26,27] represent erosion rates determined from CRN concentrations in fluvial sediments. A single bedrock erosion rate (25 m My^{-1}) was also measured by Brown et al. [26]

[a] Values represent single measurements.

[b] From CRN concentrations in fluvial sediments.

2. Study area and sampling sites

2.1. Study area

We have measured ^{10}Be and ^{26}Al concentrations from bare bedrock outcrops on summits in four Western U.S. mountain ranges: the Beartooth, Wind River, Front Range, and Sierra Nevada ranges. These ranges have several common characteristics. First, crystalline bedrock (granite or gneiss) is abundant at the highest elevations in each range. Other rock types (schist) are also abundant in the Front Range. Second, valleys were intermittently glaciated during the Pleistocene [16]. Third, many of the highest peaks and ridges in each range are capped by extensive summit flats that show no evidence of past glaciation. We collected samples from these summit flats.

2.2. Summit flats

We have observed many common features among summit flats in these four ranges. Summit flats, which are up to several km^2 in area, are largely convex with uniform curvature, and display unchannelled, low angle (typically 2–3°, maximum 10°) hillslopes up to 1 km long. A regolith thickness of 1–2 m is common. At the edges of summit flats, the regolith commonly feathers to zero, exposing a several meter wide bare bedrock bench. Cliffs several hundred meters high separate the edges of these surfaces from the glaciated troughs below. Hillslopes appear to be dominated by periglacial processes; sorted nets and stripes, felsenmeer and nivation hollows are common.

We recognize no evidence of prior glaciation on any of the summit flats, except in the Sierra Nevada, where Gillespie [17] noted evidence for possible ancient glaciations. Glacial striations and erratic boulders are absent. Boulders composed of a distinctive lithology can be traced to nearby, upslope bedrock sources. Summit flats are much smoother than the surfaces of the glaciated troughs below, where roche moutonée, other bedrock bumps, and overdeepenings ornament and complicate the broadly u-shaped valley floors. The bedrock surface underlying summit flats, which is exposed in canyon walls, is smooth; that is, it is not simply a rough bedrock landscape mantled by a smoothing regolith. There is also no evidence of either past or modern fluvial channelization. The low slopes of summit flats inhibit erosion by discrete landslides. Cliff retreat at the edges of summit flats reduces their area but does not lower the surface elevation. Because of the absence of glacial, fluvial, or landsliding processes, summit flat lowering is primarily the result of periglacial creep. The summit flat lowering rate is

Fig. 1. Summit flat tor in the Wind River Range. Tor is about 5 m high. The accumulation of unattached blocks around the base of the tor is common. The presence of these blocks suggests that tors do not erode steadily, but erode instead by a series of finite steps or chips.

limited by the bedrock weathering rate because periglacial creep is only capable of transporting unconsolidated material. Therefore, the bare bedrock weathering rates we report below are a proxy for the erosion rate of entire summit flats.

We collected samples for CRN analysis from tors (bedrock knobs that protrude through the regolith mantle) and large boulders, both of which are common on summit flats (Fig. 1). The tors are most frequently located along the crests and edges of the flats. Most of the tors are several meters high (with some up to 25 m) and ~5–10 m wide. Vertical and horizontal joint sets, with ~0.2–2 m spacing, disrupt all of the tors we examined. Numerous blocks, which have become unattached from the bedrock along joint surfaces, blanket the tops and flanks of tors. These blocks have toppled into various orientations and extend tens of meters from the tors in an apron of felsenmeer. The bedrock surface of tors is frequently defined by joint planes, which can be traced beneath adjacent bedrock that remains intact. The dimensions, orientations, and distribution of the unattached blocks and the presence of joint planes at the bedrock surface both suggest that vertical and horizontal erosion of tors proceeds by the removal of distinct joint blocks. Minor amounts of small clasts and sand indicate that erosion by granular disintegration occurs, but is far less important than the removal of blocks. Most bedrock surfaces lack relief at the centimeter and finer scales, suggesting that dissolution and ventifaction are not effective erosion processes. Because the rock surfaces we sampled appear to be actively eroding, we interpret CRN concentrations in terms of erosion rates, rather than surface exposure ages.

3. Theoretical background

CRNs are formed when target nuclei are bombarded by high-energy cosmic ray particles [18]. Silicon and stable aluminum are potential target nuclei for in situ production of ^{26}Al ($t_{1/2} = 0.7$ Ma), while oxygen is the most common target nucleus for in situ production of ^{10}Be ($t_{1/2} = 1.5$ Ma). The production of CRNs within solids decreases exponentially with depth:

$$P(z) = P_o e^{-z/z^*} \quad (1)$$

where the scale length, $z^* = \Lambda/\rho$, is the ratio of the absorption mean free path (Λ) of ~155–160 g cm^{-2} and the density of the solid (ρ) [19,20].

Assuming that the production rate at a particular location is steady through time, the rate of change in concentration of a CRN can be described by the differential equation:

$$\frac{dN}{dt} = P(z) - \lambda N(t) \quad (2)$$

where N(t) is the nuclide concentration (atoms g^{-1}) history, P(z) is the production rate (atoms g^{-1} yr^{-1}) profile with depth, z, and $\lambda = \ln 2/t_{1/2}$ is the nuclide decay constant.

For a surface eroding at a constant or steady rate, $\varepsilon(t) = \bar{\varepsilon}$, Eq. (2) can be solved analytically to yield the surface concentration of a spallation-produced CRN, such as ^{10}Be or ^{26}Al [1,2]:

$$N(0) = \frac{P_o}{(\epsilon/z^*) + \lambda} \quad (3)$$

Eq. (3) can be rewritten to solve for the 'steady-state' erosion rate. While a steady-state erosion rate can be calculated for any rock surface, the calculated rate might not reflect the true outcrop erosion rate if the steady erosion assumption ($\varepsilon(t) = \bar{\varepsilon}$) is invalid. The steady erosion assumption is valid when the erosion rate is constant on the timescale in which CRNs have accumulated at the surface ($z^*/\varepsilon \approx 10^4$–$10^5$ y). The steady erosion assumption does not require that erosion is constant on shorter timescales.

In addition to the steady erosion assumption, two other assumptions must be made when erosion rates are deduced from CRN concentrations: (1) the surface production rate is constant through time; and (2) steady erosion has persisted for long enough ($1 \gg 1/[(\varepsilon/z^*) + \lambda]$) that the surface concentration has reached the steady-state value [2]. The first assumption is only generally valid because variations in the strength of the Earth's magnetic field modulate the surface production rate [21]. We do not address these variations here. The second assumption is not valid in many settings because some geomorphic processes (glacial erosion, mass wasting, etc.) remove thicknesses of material greater than the attenuation depth for CRN production, z^*. This exposes rock at the surface that has significantly lower CRN concentration. Even for rapidly eroding outcrops ($\varepsilon > 10$ m

My $^{-1}$), the steady-state value is only approached $\sim 10^5$ yr after such an event. Therefore, CRN erosion rates are commonly considered to be maximum estimates of the true outcrop erosion rate. We apply this convention to our erosion rate interpretations.

4. Methods

4.1. Field methods

We collected samples from the tops of tors and from the tops of the largest blocks surrounding tors on summit flats (Table 2). We selected tors and boulders that had broad, smooth, and nearly horizontal upper surfaces in order to simplify corrections for exposure geometry. Samples were only collected from surfaces that extended for > 1 m at a similar elevation in all directions. The elevation and latitude of sample sites were determined from 1:24,000 topographic maps. We measured the vertical angles to the horizon with a hand held inclinometer. We also measured the strike and dip of outcrop surface and the thickness of the sample collected.

4.2. Estimation of production rates

Local surface production rates, P_0, were calculated using the latitude–elevation coefficients of Lal

Table 2
^{10}Be and ^{26}Al data for summit flat samples

Sample	Rock type	Elevation (m)	Concentration (10^6 atoms/g SiO_2)		Ratio ^{26}Al/^{10}Be	Maximum erosion rate (m/My)		Effective age (ky)	
			^{10}Be	^{26}Al		^{10}Be	^{26}Al	^{10}Be	^{26}Al
Wind River, WY									
Wr-4	gneiss	3597	6.31 ± 0.17	32.0 ± 0.94	5.07 ± 0.20	4.96 ± 1.11	6.40 ± 1.53	105 ± 21	84 ± 17
Wr-5	gneiss	3597	3.85 ± 0.08	22.8 ± 1.00	5.92 ± 0.29	8.29 ± 1.81	9.22 ± 2.18	64 ± 13	60 ± 12
Wr-9	granite	3737	3.94 ± 0.09	22.8 ± 0.96	5.79 ± 0.28	8.78 ± 1.91	10.04 ± 2.36	60 ± 12	55 ± 11
Wr-11	granite	3633	7.58 ± 0.20	42.8 ± 1.39	5.65 ± 0.24	4.17 ± 0.94	4.74 ± 1.16	124 ± 25	110 ± 22
Wr-18	granite	3737	3.94 ± 0.22	21.1 ± 0.53	5.36 ± 0.33	8.78 ± 1.97	10.89 ± 2.52	61 ± 13	51 ± 10
Wr-19 [a]	granite	3688	3.26 ± 0.07	18.6 ± 0.71	5.71 ± 0.25	10.37 ± 2.25	12.11 ± 2.81	52 ± 10	46 ± 9
Wr-20 [a]	granite	3688	11.20 ± 0.25	61.4 ± 2.39	5.48 ± 0.25	2.85 ± 0.65	3.25 ± 0.84	176 ± 36	153 ± 31
mean						6.9 ± 2.8	8.1 ± 3.3	92 ± 46	80 ± 39
Beartooth, MT									
Bt-2	granite	3304	4.84 ± 0.13	31.3 ± 1.92	6.47 ± 0.43	5.67 ± 1.26	5.65 ± 1.40	92 ± 19	94 ± 20
Bt-3 [b]	granite	3316	1.83 ± 0.09	13.1 ± 1.34	7.16 ± 0.81	15.57 ± 3.43	14.45 ± 3.63	35 ± 7	39 ± 8
Bt-4 [b]	granite	3316	2.81 ± 0.12	24.4 ± 1.88	8.68 ± 0.76	10.06 ± 2.22	7.52 ± 1.87	53 ± 11	72 ± 16
Bt-5 [b]	granite	3316	1.98 ± 0.09	10.3 ± 1.11	5.20 ± 0.61	14.43 ± 3.17	18.63 ± 3.30	37 ± 7	49 ± 10
Bt-6 [b]	granite	3316	4.58 ± 0.14	25.5 ± 2.03	5.57 ± 0.47	6.09 ± 1.35	7.17 ± 1.79	86 ± 17	76 ± 16
mean						10.3 ± 4.6	10.7 ± 5.6	61 ± 27	63 ± 27
Front Range, CO									
Tr-1	schist	3575	4.65 ± 0.15	2.7 ± 1.21	5.76 ± 0.32	6.86 ± 1.52	7.82 ± 1.86	77 ± 16	7014
Tr-2	schist	3725	5.14 ± 0.14	31.1 ± 1.31	6.05 ± 0.31	6.14 ± 1.36	6.62 ± 1.59	86 ± 17	82 ± 17
Rp-1 [a]	granite	3713	3.29 ± 0.14	22.2 ± 2.01	6.75 ± 0.68	8.96 ± 1.98	8.74 ± 1.49	59 ± 12	64 ± 8
Ft-2	granite	3734	4.85 ± 0.16	28.6 ± 1.24	5.90 ± 0.32	6.60 ± 1.46	7.32 ± 1.75	80 ± 16	74 ± 15
mean						7.1 ± 1.2	7.6 ± 0.9	75 ± 11	72 ± 7.9
Sierra Nevada, CA									
Lp-1 [a]	granite	3750	11.4 ± 0.3	78.2 ± 2.14	6.86 ± 0.26	2.43 ± 0.57	2.09 ± 0.57	204 ± 41	220 ± 44
Lp-2 [a]	granite	3750	5.9 ± 0.2	41.3 ± 1.04	6.96 ± 0.30	4.93 ± 1.11	4.47 ± 1.10	106 ± 21	116 ± 23
Lp-3 [a]	granite	3750	13.2 ± 0.3	81.2 ± 3.02	6.15 ± 0.28	2.07 ± 0.49	1.99 ± 0.55	236 ± 48	228 ± 46
mean						3.1 ± 1.6	2.9 ± 1.4	182 ± 68	188 ± 62

In addition to maximum erosion rates, effective ages ($T_{eff} = N(0)/P(0)$; [2]) are also shown. All errors are 1σ standard deviations. Concentration and ratio error calculations include propagated ratio and concentration errors measured during AMS, FAAS, and ICP/MS analyses. Erosion rate and effective age calculations include propagated errors (estimated) from the production rate (10%), flux attenuation length (5%) and rock density (5%)

[a] Samples from boulders, not tors.

[b] Samples from the same tor.

[2], the sea level high-latitude ^{10}Be production rate (4.9 atom g^{-1} yr^{-1}) of Clark et al. [21], and the ^{26}Al–^{10}Be sea-level production rate ratio (6.1) of Nishiizumi et al. [22]. The effects of topographic shielding are negligible. For all samples, the topographic shielding factor [22] was between 0.99 and 1.00. The mean production rate, P_o', over the depth interval represented by the thickness of the sample, z_s, was calculated by integrating the production profile with depth:

$$P_o' = \frac{P_o}{z_s}\int_0^{z_s} P_o \exp(-z/z^*)\,dz \quad (4)$$

Because all samples were < 5 cm thick, the mean production rate over the sample thickness was always within a few percent of P_o.

4.3. Laboratory methods

We crushed and sieved samples to a size of 1.25–2.25 ϕ and then separated quartz grains from other minerals with heavy liquid and magnetic separation techniques. Organics, Fe and Mg oxides, and carbonates were eliminated by heating for 24 h in a solution of 30% HCl and 1% H_2O_2. We then leached samples (> 6 times) for 24 h in a 1% HF + 1% HNO_3 solution to remove any remaining non-quartz grains, and to assure elimination of any atmospherically produced 'garden variety' ^{10}Be.

We added 0.5 mg of stable Be and Al to a 10–20 g quartz sample and dissolved the sample in concentrated HF. Stable beryllium and aluminum concentrations were determined by flame atomic absorption spectroscopy (FAAS) and by inductively coupled plasma mass spectrometry (ICP/MS) on an aliquot of the sample. Al and Be were separated by ion chromatography, precipitated as metal hydroxides, and then oxidized over a flame. In the Al_2O_3 or BeO form, the ratio of the radionuclide to the stable isotope was determined by accelerator mass spectrometry (AMS) at the LLNL/CAMS facility [23,24].

5. Results

The mean erosion rate from all summit flat samples is 7.6 ± 3.9 m My^{-1} (Fig. 2, Table 2). Because the rock surfaces we sampled may not yet have

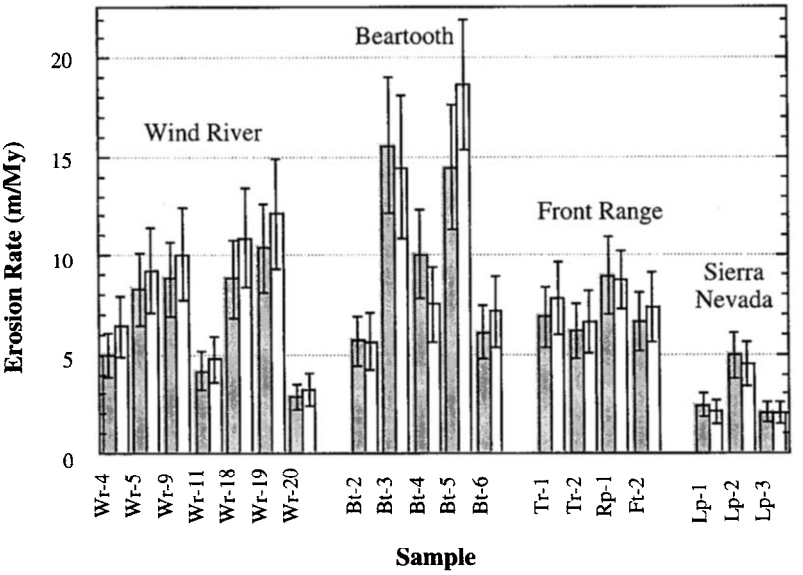

Fig. 2. ^{10}Be (shaded) and ^{26}Al maximum erosion rates from summit flat tors and boulders. The rock type, elevation, and sample type (tor or boulder) of each measurement is shown in Table 2. Error bars for each sample are 1σ standard deviations, and include propagated errors from the production rate, flux attenuation length, rock density, and ratio and concentration measurements. The mean erosion rate from each mountain range is shown in Table 2. The mean erosion rate for all samples is 7.6 ± 3.9 m My^{-1}.

reached steady-state CRN concentrations following some exposure event in the past, we consider this rate to be a maximum. The variability in steady-state erosion rates within each mountain range is high; the standard deviation is ~20–50% of the mean. In the following section, we show that this variability could be the result of episodic erosion. Mean erosion rates also vary among the mountain ranges. The mean value from the Beartooth Range is highest (based upon ^{10}Be: 10.3 ± 4.6 m My^{-1}) while the mean value from the Sierra Nevada is lowest (^{10}Be: 3.1 ± 1.6 m My^{-1}) (Table 2). We cannot draw any conclusions about differences in bedrock weathering rates between the four mountain ranges because our sampling method varied from range to range. For example, all three samples from the Sierra Nevada were taken from large boulders, while four of the five samples from the Beartooth Range were taken from a single tor (Table 2).

To compare our results with those from previous CRN erosion rate studies (Table 1), we must adjust for differences in the sea-level, high-latitude production rate used in erosion rate calculations. In most previous studies, a ^{10}Be production rate of 6.0 a g^{-1} y^{-1} was used [22], while here we use a rate of 4.9 a g^{-1} y^{-1} [21]. We must therefore raise our erosion rate values by ~20% to make a direct comparison to previous results. Assuming a ^{10}Be production rate of 6.0 a g^{-1} y^{-1}, the mean erosion rate from all summit flat samples becomes 9.1 ± 4.7 m My^{-1}. This value is very similar to the CRN erosion rates measured in most other non-arid regions, across a variety of lithologies (Table 1). This value is noticeably lower than the erosion rates reported by Nishizumi et al. [5] from alpine sites in the Grand Tetons and the Himalaya, but is similar to the single measurement from Mt. Evans in Colorado.

5.1. Frost weathering efficiency

Based upon this comparison, bare bedrock is not weathered into transportable material more rapidly in alpine than in other environments, even though frost action should be active nearly year round in this setting [6,15]. This suggests that the net effect of all weathering processes is roughly equal between the different environments in which CRN erosion rates have been measured, excluding extremely arid regions. Frost action must not transform bedrock into transportable material faster than other weathering processes, unless other weathering processes which are important elsewhere are suppressed in alpine environments. Alternatively, frost action may weather bedrock very rapidly in certain areas of alpine environments, but not at the locations from which we sampled. Regardless of whether frost action is driven by freeze–thaw cycling [15] or sustained sub-zero temperatures [6], ample water is required for sub-zero temperatures to break apart bedrock. None of our samples were taken from locations along, or at the convergence of, surface or subsurface water flowpaths. These sites represent the driest points in the landscape, where the influx of water is limited only to atmospheric sources. At these sites frost action may be inhibited by the relatively dry conditions. We cannot compare our results to observations obtained in previous frost weathering studies because these efforts have focused on the retreat rate of near-vertical rock walls [11–14].

5.2. Spatial variability of erosion

Bierman [1] noted that CRN-deduced bedrock erosion rates are slower than typical basin-averaged denudation rates in similar settings, which are typically ~50 m My^{-1} [25]. Various methods have been used to measure these basin-averaged rates, including the analysis of CRN concentrations in sediment leaving a basin [26,27]. Our results show a similar disparity. For example, the denudation rate from the glaciated portion of the Wind River Range that includes several of our sample locations is 110 m My^{-1} [28]. We expect similarly high basin-averaged denudation rates from the other three ranges sampled, because erosion rates from high-relief, glaciated regions are typically very rapid [28,29].

If the bedrock erosion rates we have measured are representative of the rate at which entire summit flats are lowered by erosion, then relief in these mountains is presently increasing by ~100 m My^{-1}, because peaks are eroding more slowly than adjacent valleys. The rate of relief production estimated here is important because it controls the rate at which peak elevations will increase due to the isostatic response to erosional unloading [30–32]. Our point estimates of bare-bedrock erosion may be accurate

indicators of summit flat erosion rates because both tor and summit flat lowering appear to be limited by bedrock weathering (discussed above). However, most of the bedrock on summit flats is covered by shallow (1–2 m) regolith, which may alter the rate at which bedrock is converted into transportable material [33,34]. In future work we will report on measurements of the buried-bedrock weathering rate (or regolith production rate) using CRNs in order to assess whether the bedrock lowering rates we have measured are representative of entire summit flats.

6. Modelling episodic erosion

A model which represents a sample's exposure history is required to deduce geologic information from CRN concentrations [1]. If the assumptions of a model are not valid, the resulting geologic information is likely to be incorrect [1,2,35–37]. When erosion rates are deduced from CRN concentrations, it is assumed that erosion is steady on the CRN timescale, $z^*/\varepsilon \approx 10^4$–$10^5$ yr [1,2]. This assumption is likely invalid in most environments and for most lithologies. Frost action, chemical dissolution, fire spallation and other processes break apart bedrock into transportable fragments, frequently along joints or bedding planes. Because fragment depths, L, are commonly the same order of magnitude as z^*, erosion is episodic on the CRN timescale ($L/\varepsilon \approx z^*/\varepsilon$), and the steady erosion assumption is invalid. Our field observations indicate that tors and boulders in alpine environments erode by the episodic removal of finite blocks or chips. Episodic erosion has also been observed in arid environments subjected to range fires [35].

$^{26}Al/^{10}Be$ ratios can only be used to assess the validity of the steady erosion assumption when λ_{Be}, $\lambda_{Al} \geq \varepsilon/z^*$ ($\varepsilon < 1$ m My^{-1}). Erosion this slow is atypical, and has only been measured in two extremely arid locations (Table 1). When $\varepsilon > 1$ m My^{-1}, which is the case for most CRN-deduced erosion rates (Table 1), the steady-erosion assumption cannot be tested. Regardless of the erosion rate, the removal of a rock fragment lowers the ^{10}Be concentration but does not significantly alter the $^{26}Al/^{10}Be$ ratio (Fig. 3). When erosion is slow (^{10}Be concentration is high), a sample plots far below the

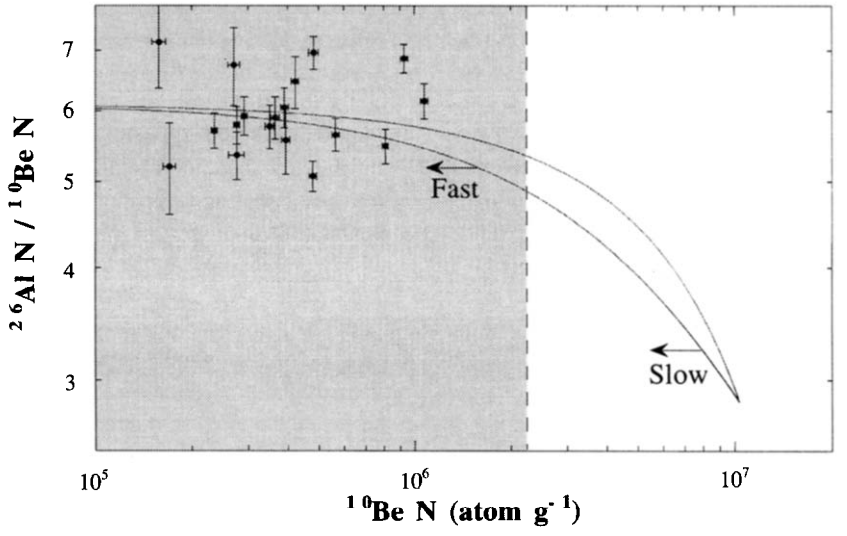

Fig. 3. The steady-erosion island is bounded by the no erosion (top) and steady-erosion (bottom) lines. Samples move along trajectories shown by arrows (examples for fast and slow erosion) immediately following the removal of a rock chip. Within the shaded region (fast erosion; $\varepsilon > 1$ m My^{-1}), the steady-erosion assumption cannot be tested (within analytical uncertainty) because the slope of the steady-state erosion line is almost zero. The $^{26}Al/^{10}Be$ ratio vs. ^{10}Be concentration for summit flat samples are plotted. ^{10}Be concentrations are normalized to sea level, high-latitude production rates. Erosion is too fast for the steady-erosion assumption to be tested for any of the summit flat samples.

steady-erosion island following an episodic erosion event. However, when erosion is fast, samples that have experienced episodic erosion plot very close to the steady-erosion island because the slope of the island's lower boundary is near zero for low ^{10}Be concentrations (Fig. 3). In this case, one cannot distinguish between episodic and steady erosion within reasonable measurement uncertainty. Even without the considerable scatter in our ^{26}Al/^{10}Be ratios, which probably results from analytical errors, we would be unable to test if erosion was steady (Fig. 3). If the fundamental assumption of the erosion rate model cannot be tested, which is the case in most geomorphic environments, it is critical to estimate the potential errors produced by episodic erosion.

We quantify the expected variability in steady-state erosion rates produced by episodic erosion using a finite-difference model. In order to address episodic erosion in a broad range of environments, we vary the chip depth from the mineral grain scale to that which we have observed in alpine settings (tens of centimeters). We also vary the long-term mean erosion rate, which is the rate at which the outcrop surface is lowered averaged over many episodic chipping events. We apply our model results to the erosion rates reported above, in order to evaluate the potential impacts of episodic erosion on our measurements. In addition, we suggest a sampling plan that minimizes errors resulting from episodic erosion.

Lal [2] modeled a particular case of non-steady erosion, in which the outcrop erodes at a constant rate before and after a single chip is removed (Fig.

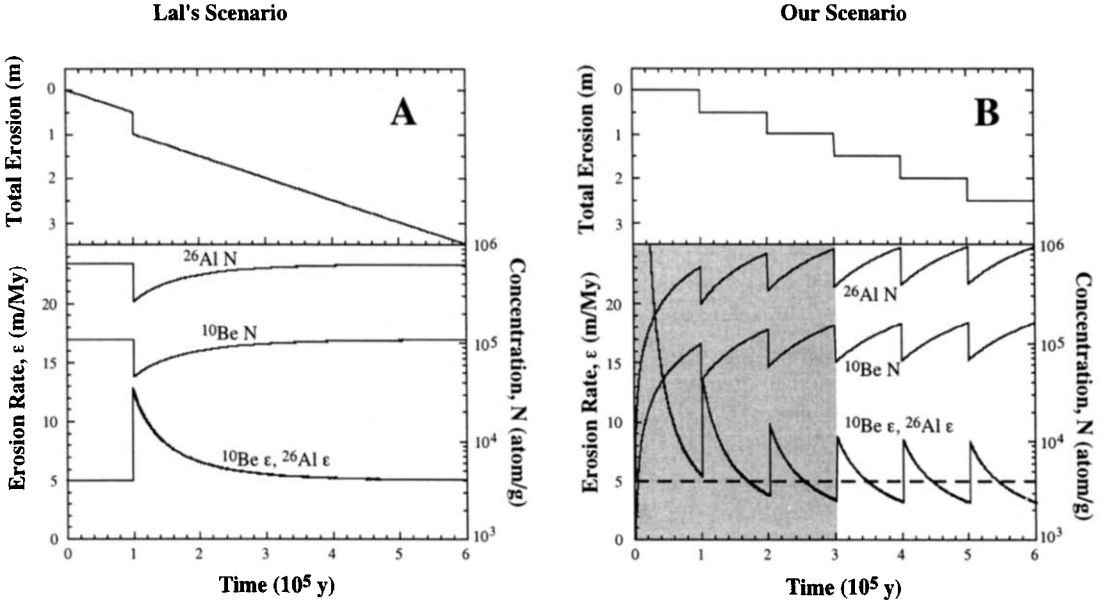

Fig. 4. (a) Lal's [2] simulation of non-steady erosion: the outcrop erodes at a constant rate (5 m My^{-1}) before and after a single 15 cm chip is removed at time $\approx 1 \times 10^5$ y (top panel). The ^{10}Be and ^{26}Al concentrations of the rock surface and steady-state erosion rates are shown throughout the simulation (bottom panel). This erosion history only elevates the steady-state erosion rate above the background outcrop erosion rate. For cases when $\varepsilon/z^* > \lambda$ (rapid erosion), decay is unimportant and the ^{10}Be- and ^{26}Al-deduced steady-state erosion rates are identical. $z^* = 0.6$ m. (b) Model simulation of an outcrop that erodes by repeated cycles consisting of the removal of a 15 cm chip followed by a period of no erosion (top panel). The mean erosion rate is 5 m My^{-1}. Resulting model history of CRN concentrations from surface samples and the associated steady-state erosion rates are shown in the bottom panel. After the model reaches steady state ($> 3 \times 10^5$ y; shaded region), the steady-state erosion rate varies between being greater and less than the true mean erosion rate (dashed line). The maximum steady-state erosion rate is further from the mean than the minimum. However, the mean steady-state erosion rate is nearly identical to the actual mean rate because the steady-state erosion rate is less than the mean for more than half of the chipping cycle. $z^* = 0.6$ m.

4a). Directly following the chipping event, the CRN concentration at the surface of the outcrop drops to the steady-state erosion concentration found at the chip depth. The surface CRN concentration subsequently increases until the original steady-state surface concentration is attained. The steady-state erosion rate increases immediately following chip removal, and subsequently falls back to the steady-state erosion value at which the outcrop is being lowered. Lal [2] concluded that steady-state erosion rates should be considered maximum values in terms of the effects of chipping, because non-steady erosion raises the steady-state erosion rate above the actual mean erosion rate. This conclusion is only valid for the erosion history modeled by Lal [2], which does not adequately depict the episodic erosion observed in alpine and other environments.

We explore the following episodic erosion scenario using a finite-difference model: an outcrop surface erodes by the removal of chips of constant depth, L, each erosion event separated by an interval, t_c (Fig. 4b). The mean erosion rate, $\bar{\varepsilon}$, is then $\bar{\varepsilon} = L/t_c$. Initially, CRN concentration is 0.0 at all depths. Models are run to steady state and time steps are $< 0.01 t_c$. The ^{10}Be and ^{26}Al steady-state erosion rate that would be deduced by sampling the instantaneous surface is calculated according to Eq. (3) at each time step. The maximum, minimum, mean and standard deviation of this steady-state erosion rate are calculated for each chipping cycle. We vary both the chip depth and mean erosion rate in different model runs.

The CRN concentrations at the rock surface drop immediately following a chipping event and subsequently increase; the steady-state erosion rates therefore rise following chip removal and subsequently decrease (Fig. 4b). After the transience associated with model initialization has ended, the steady-state erosion rates vary between being greater than (following a chipping event) and less than (prior to a chipping event) the actual mean outcrop erosion rate. Therefore, a single steady-state erosion rate measured from an outcrop that is eroding episodically by finite chips may be either greater or less than the actual mean erosion rate of the rock surface, depending on when in the chipping cycle the sample is taken. Considering steady-state erosion rates as maximums with respect to episodic erosion, as suggested by Lal [2], is therefore inappropriate for erosion histories similar to those observed in alpine and other settings.

6.1. Magnitude of the error

When erosion is rapid ($\varepsilon/z^* > \lambda$; decay is negligible), as is the case for our samples and most previously measured CRN erosion rates, an analytical expression exists for the minimum and maximum steady-state erosion rates throughout a chipping cycle. The difference between the maximum and minimum possible CRN concentrations is set entirely by the depth, L, of the chip removed:

$$N_{min} = N_{max} e^{-L/z^*} \tag{5}$$

In the absence of decay, the surface CRN concentration increases linearly between chipping events. Therefore, $(N_{max} - N_{mean})$ must equal $(N_{mean} - N_{min})$. The absolute value of N_{max} or N_{min} can be calculated based on this equality, and on the mean CRN concentration, $N_{mean} = P_0 z^*/\bar{\varepsilon}$:

$$N_{max} = \frac{P_0 z^*}{\bar{\varepsilon}} \frac{2}{(1 + e^{-L/z^*})} \tag{6}$$

The minimum and maximum steady-state erosion rates, normalized by the actual mean erosion rate, become:

$$\frac{\varepsilon_{min}}{\bar{\varepsilon}} = \frac{1 + \exp(-L/z^*)}{2};$$

$$\frac{\varepsilon_{max}}{\bar{\varepsilon}} = \frac{1 + \exp(-L/z^*)}{2e^{-L/z^*}} \tag{7}$$

The magnitude of the variation in steady-state erosion rate about the mean erosion rate increases with larger chip depth (Fig. 5). As the chip depth diminishes, the error associated with episodic erosion approaches zero; the steady-state solution is exact. When chip depths are $> \sim 10$ cm, measuring a single erosion rate from a study area could result in large errors if the sample was collected near the start or end of a chipping cycle. For the combination of chip length (~ 0.1–0.4 m) and mean erosion rate (~ 7 m My^{-1}) we most frequently observed in the field, the greatest possible errors resulting from a single measurement would be ~ 25–50% (Fig. 5). When erosion is slow ($\varepsilon/z^* < 1$ m My^{-1}), the

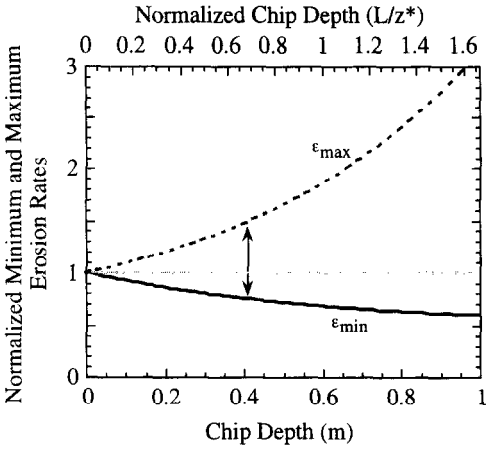

Fig. 5. Dependence of the minimum (solid line) and maximum (dashed line) steady-state erosion rates, normalized against the steady state erosion rate (gray line), on the chip depth. The range of possible steady-state erosion rates for a chip depth of 0.4 m, typical of our high surface tors, is shown by the arrows, the maximum steady-state rate being ~ 50% above the actual mean, the minimum ~ 25% below it. $z^* = 0.6$ m.

magnitude of the variation in steady-state erosion rate also increases with slower mean outcrop erosion rate (not shown).

By calculating the variability represented by the full population of steady-state erosion rates that exist throughout a simulated chipping cycle, we can directly compare errors associated with episodic erosion to other errors involved in deducing erosion rates from CRN concentrations. The variability of steady-state erosion rates increases for larger chip depths (Fig. 6). When erosion is slow ($\bar{\varepsilon}/z^* < \lambda$), the variability also increases with decreasing erosion rates. Regardless of the mean outcrop erosion rate, non-steady erosion produces > 20% variability (1σ deviation) in steady-state erosion rates around the actual mean when the chip depth is $\geq \sim 0.25$ m (Fig. 6). Therefore, for the chip depths we observed in the field, the errors resulting from non-steady erosion should be greater than both measurement and production rate errors, ~ 5% and ~ 20%, respectively [21]. A sampling strategy that minimizes these errors is needed.

6.2. Sampling scheme

While large errors may result from single measurements, taking the mean value of many steady-state erosion rate measurements should provide a more accurate estimate of the actual mean erosion rate. This is the case because fluctuations in the steady-state erosion rate, ε_{ss}, are equally distributed about the actual mean erosion rate (Fig. 4b):

$$\frac{1}{t_c}\int_0^{t_c}(\varepsilon_{ss} - \varepsilon)\,dt \approx 0 \qquad (8)$$

The larger difference between the maximum steady-state erosion rate and the mean $(\varepsilon_{max} - \bar{\varepsilon}) > (\bar{\varepsilon} - \varepsilon_{min})$ is offset by the steady-state erosion rate being less than the mean for a majority of the chipping cycle (Fig. 4b). The difference between the mean of many steady-state erosion rates and the actual ero-

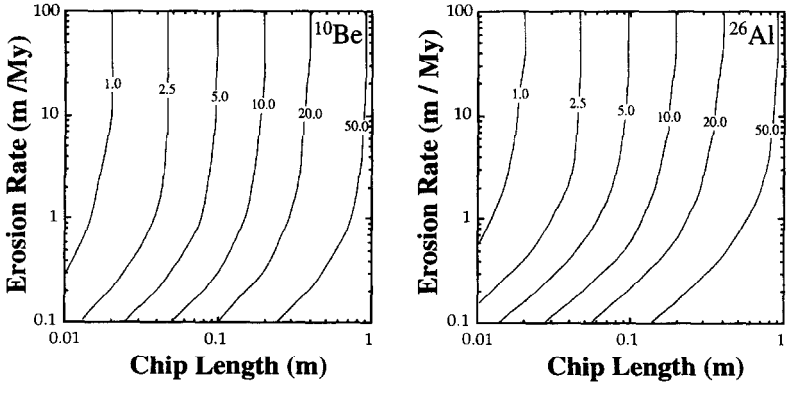

Fig. 6. Variability (1σ percent standard deviation) in steady-state erosion rates throughout repeated chipping cycles, for varying chip depth and mean erosion rate. Lines of equal percent standard deviation are shown. For rapid erosion, variability is constant for different erosion rates (lines are vertical). $z^* = 0.6$ m.

sion rate is $< 1\%$ for most combinations of mean erosion rate and chip depth. For combinations of slow erosion and large chip depth, the difference is as large as $\sim 5-10\%$. Therefore, if enough samples are analyzed from a single area, and chipping is not synchronous for the outcrops sampled, the mean value of the measured steady-state erosion rates should provide a good estimate of the actual mean outcrop erosion rate, especially if erosion is fast. Because of this relationship, we feel confident that our measured mean erosion rates (each based on many samples) from each mountain range are accurate indicators of the true bare-bedrock erosion rates, even though episodic erosion is common in our study area.

7. Conclusions

(1) The maximum mean bare-bedrock erosion rate from summit flats in four Western U.S. mountain ranges is 7.6 ± 3.9 m My^{-1}. This rate is much slower than expected basin-averaged erosion rates within these mountains, which suggests that relief may be increasing if summit flat erosion is limited by bedrock weathering.

(2) The erosion rates we report here are very similar to CRN erosion rates measured in other environments. This suggests that the efficiency of all weathering processes in converting bare-bedrock into transportable material in different environments is similar, excluding very arid environments. Frost action does not appear to accelerate mechanical weathering of bare-bedrock surfaces in alpine environments.

(3) For an outcrop that erodes by a series of chips, the steady-state erosion rate varies between being greater and less than the actual mean erosion rate of the outcrop, the variability scaled primarily by the thickness of the chips. The steady-state erosion rate of a single sample may be very different from the actual erosion rate; however, the mean of many steady-state erosion rates can provide an accurate estimate of the actual mean outcrop erosion rate.

Acknowledgements

We thank Gregory Dick, Robert Stollard and an anonymous reviewer for constructive criticisms. This work was supported by the Topography and Surface Change Program of the National Aeronautics and Space administration and a National Defense Science and Engineering graduate fellowship to E. Small. *[MK]*

References

[1] P.R. Bierman, Using in situ cosmogenic isotopes to estimate rates of landscape evolution: A review from the geomorphic perspective, J. Geophys. Res. 99 (1994) 13885–13896.

[2] D. Lal, Cosmic ray labeling of erosion surfaces: *In situ* production rates and erosion models, Earth Planet. Sci. Lett. 104 (1991) 424–439.

[3] K. Nishiizumi, C.P. Kohl, J.R. Arnold, J. Klein, D. Fink, R. Middleton, Cosmic ray produced ^{10}Be and ^{26}Al in Antarctic rocks: exposure and erosion history, Earth Planet. Sci. Lett. 104 (1991) 440–454.

[4] P.R. Bierman, J. Turner, Be-10 and Al-26 evidence for exceptionally low rates of Australian bedrock erosion and the likely existence of pre-Pleistocene landscapes, Quat. Res. 44 (1995) 367–377.

[5] K. Nishiizumi, C.P. Kohl, J.R. Arnold, R.I. Dorn, J. Klein, D. Fink, R. Middleton, D. Lal, Role of in situ cosmogenic nuclides ^{10}Be and ^{26}Al in the study of diverse geomorphic processes, Earth Surf. Processes Landforms 18 (1993) 407–425.

[6] J. Walder, B. Hallet, A theoretical model of the fracture of rock during freezing, Geol. Soc. Am. Bull. 96 (1985) 336–346.

[7] B. Hallet, J.S. Walder, C.W. Stubbs, Weathering by segregation ice growth in microcracks at sustained sub-zero temperatures: Verification from an experimental study using acoustic emissions, Permafrost Periglacial Processes 2 (1991) 283–300.

[8] J.P. Coutard, B. Francou, Rock temperature measurements in two alpine environments: implications for frost shattering, Arct. Alp. Res. 21 (1989) 399–416.

[9] N. Matsuoka, Diurnal freeze–thaw depth in rockwalls: field measurements and theoretical considerations, Earth Surf. Processes Landforms 19 (1994) 423–435.

[10] R.S. Anderson, Shallow thermal profiles in bedrock, Laramie Range, Wyoming, and their implications for the frost weathering of rock, EOS Trans. Am. Geophys. Union 76 (1995) 276.

[11] B.H. Luckman, Rockfalls and rockfall inventory data: Some observations from Surprise Valley, Jasper National Park, Canada, Earth Surf. Processes 1 (1976) 287–298.

[12] G.R. Douglas, Magnitude frequency study of rockall in Co. Antrim, N. Ireland, Earth Surf. Processes 5 (1980) 123–129.

[13] B.D. Fahey, T.H. Lefebure, The freeze–thaw weathering regime at a section of the Niagara Escarpment on the Bruce Peninsula, southern Ontario, Canada, Earth Surf. Processes Landforms 13 (1988) 293–304.

[14] N. Matsuoka, The rate of bedrock weathering by frost action: field measurements and a predictive model, Earth Surf. Processes Landforms 15 (1990) 73–90.
[15] J.P. McGreevy, W.B. Whalley, Rock moisture content and frost weathering under natural and experimental conditions: A comparitive discussion, Arct. Alp. Res. 17 (1985) 337–346.
[16] S.C. Porter, K.L. Pierce, T.D. Hamilton, Late Wisconsin mountain glaciation in the western United States, in: S.C. Porter (Ed.), Late Quaternary Environments of the United States, vol. 2, The Late Pleistocene, 1982, pp. 71–111.
[17] A.R. Gillespie, Quaternary glaciation and tectonism in the southeastern Sierra Nevada, Inyo County, California, Ph.D. Thesis, California Inst. Technology, 1982.
[18] D. Lal, B. Peters, Cosmic-ray produced radioactivity on the earth, in: S. Flugge (Ed.), Handbook of Physics, Springer, Berlin, 1967, pp. 551–612.
[19] E.T. Brown, E.J. Brook, G.M. Raisbeck, F. Yiou, M.D. Kurz, Effective attenuation of cosmic rays producing ^{10}Be and ^{26}Al in quartz: Implications for exposure dating, Geophys. Res. Lett. 19 (1992) 369–372.
[20] K. Nishiizumi, Cosmogenic production of ^{10}Be and ^{26}Al on the surface of the Earth and underground, in: Abstracts 8th Int. Conf. on Geochronology, Cosmochronology, and Isotope Geology, U.S. Geol. Surv. Circ. 1107 (1994) 234.
[21] D.H. Clark, P.R. Bierman, P. Larsen, Improving *in situ* cosmogenic chronometers, Quat. Res. 44 (1995) 367–377.
[22] K. Nishiizumi, E.L. Winterer, C.P. Kohl, J. Klein, R. Middleton, D. Lal, J.R. Arnold, Cosmic ray production rates of ^{10}Be and ^{26}Al in quartz from glacially polished rocks, J. Geophys. Res. 94 (B12) (1989) 17907–17915.
[23] D. Elmore, F. Phillips, Accelerator mass spectrometry for measurement of long-lived radioisotopes, Science 236 (1987) 543–550.
[24] J.C. Davis, I.D. Proctor, J.R. Southon, M.W. Caffee, D.W. Heikkinen, M.L. Roberts, K.W. Moore, K.W. Turteltaub, D.E. Nelson, D.H. Loyd, J.S. Vogel, LLNL/UC AMS facility and research program, Nucl. Instrum. Methods Phys. Res. B52 (1990) 269–272.
[25] I. Saunders, A. Young, Rates of surface processes on slopes, slope retreat, and denudation, Earth Planet. Sci. Lett. 8 (1983) 473–501.
[26] E.T. Brown, R.F. Stallard, M.C. Larsen, G.M. Raisbeck, F. Yiou, Denudation rates determined from the accumulation of in situ-produced ^{10}Be in the Luquillo Experimental Forest, Puerto Rico, Earth Planet. Sci. Lett. 129 (1995) 193–202.
[27] D.E. Granger, J.W. Kirchner, R. Finkel, Spatially averaged long-term erosion rates measured from in situ-produced cosmogenic nuclides in alluvial sediment, J. Geol. 104 (1996) 249–257.
[28] F. Ahnert, Functional Relationships between denudation, relief, and uplift in large mid-lattitude drainage basins, Am. J. Sci. 268 (1970) 243–263.
[29] B. Hallet, L. Hunter, J. Bogen, Rates of erosion and sediment evacuation by glaciers: a review of field data and their implications, Glob. Planet. Change 12 (1996) 213–235.
[30] P. Molnar, P. England, Late Cenozoic uplift of mountain ranges and global climate change: chicken or egg?, Nature 346 (1990) 29–34.
[31] E.E. Small, R.S. Anderson, Geomorphically driven late Cenozoic rock uplift in the Sierra Nevada, California, Science 270 (1995) 277–280.
[32] L.D. Abbott, E.A. Silver, R.S. Anderson, R. Smith, J.C. Ingle, S.A. King, D. Haig, E. Small, J. Galewsky, W. Sliter, Measurement of tectonic surface uplift rate in a young collisional mountain belt, Nature 385 (1997) 501–507.
[33] A.M. Heimsath, W.E. Dietrich, K. Nishiizumi, R.C. Finkel, Soil production and landscape equilibrium: hillslope analysis using cosmogenic nuclides in northern California and coastal Oregon, EOS Trans. Am. Geophys. Union 77 (1996) 245–246.
[34] E.E. Small, R.S. Anderson, Erosion rates of Laramide summit surfaces: Implications for late Cenozoic increases in summit elevations, Geol. Soc. Am. Abstr. Prog. 28 (1996) A515.
[35] P.R. Bierman, A.R. Gillespie, Range fires: A significant factor in exposure-age determination and geomorphic surface evolution, Geology 19 (1991) 641–644.
[36] B. Hallet, J. Putkonen, Surface dating of dynamic landforms, Science 265 (1994) 937–940.
[37] R.S. Anderson, J.L. Repka, G.S. Dick, Explicit treatment of inheritance in dating depositional surfaces using *in situ* ^{10}Be and ^{26}Al, Geology 24 (1996) 47–51.
[38] P.R. Bierman, Cosmogenic isotopes and the evolution of granitic landforms, Ph.D. Thesis, Univ. Washington, 1993.
[39] M.D. Kurz, *In situ* production of terrestrial cosmogenic helium and some applications to geochronology, Geochim. Cosmochim. Acta 50 (1986) 2855–2862.
[40] A. Albrecht, G. Herzog, J. Klein, B. Dezfouly-Arjomandy, F. Goff, Quaternary erosion and cosmic-ray-exposure history derived from ^{10}Be and ^{26}Al produced in situ — An example from Pajarito plateau, Valles caldera region, Geology 21 (1993) 551–554.